Available online at www.sciencedirect.com
ScienceDirect
Proceedings of the Combustion Institute 32 (2009) 1253–1260
Proceedings of the Combustion Institute
www.elsevier.com/locate/proci

Effects of Lewis number and ignition energy on the determination of laminar flame speed using propagating spherical flames

Zheng Chen *, Michael P. Burke, Yiguang Ju

Department of Mechanical and Aerospace Engineering, Princeton University, Princeton, NJ 08544, USA

Abstract

The trajectories of outwardly propagating spherical flames initiated by an external energy deposition are studied theoretically, numerically, and experimentally by using hydrogen/air mixtures. Emphasis is placed on how to accurately determine the laminar flame speeds experimentally from the time history of the flame fronts for mixtures with different Lewis numbers and ignition energies. The results show that there is a critical flame radius only above which is the linear and non-linear extrapolation for flame speeds valid. It is found that the critical radius depends strongly on the Lewis number. At large Lewis numbers, the critical radius is larger than the minimum flame radius used in the experimental measurements, leading to invalid flame speed extrapolation. The results also show that there is a maximum Karlovitz number beyond which propagating spherical flame does not exist. The maximum Karlovitz number decreases dramatically with the increase of Lewis number. Furthermore, the results show that the ignition energy has a significant impact on the flame trajectories. It is found that the unsteady flame transition causes a flame speed reverse phenomenon near the maximum Karlovitz number with different ignition energies. The occurrence of flame speed reverse greatly narrows the experimental data range for flame speed extrapolation. The strong dependence of flame trajectory on ignition energy and the existence of the flame speed reverse phenomenon are also confirmed by experimental results.
Published by Elsevier Inc. on behalf of The Combustion Institute.

Keywords: Laminar flame speed; Spherical flame; Flame transition; Ignition energy; Flame speed reverse

1. Introduction

The laminar flame speed, S_u^0, is one of the most important parameters of a combustible mixture. On a practical level, it affects the fuel burning rate in internal combustion engines and the engine's performance and emissions. On a fundamental level, the flame speed is an important target for kinetic mechanism development and validation. *Accurate* determination of laminar flame speed is extremely important for the development and validation of kinetic mechanisms for gasoline and diesel surrogate fuels and alternative fuels [1–3]. In the last fifty years, great attention has been given to the development of new techniques and the improvement of existing methodologies for experimental determination of laminar flame speed, and different flame configurations have been utilized for flame speed measurement [4,5]. Among them, utilizing an outwardly propagating

* Corresponding author. Fax: +1 609 258 6233.
E-mail address: zhengc@princeton.edu (Z. Chen).

1540-7489/$ - see front matter Published by Elsevier Inc. on behalf of The Combustion Institute.
doi:10.1016/j.proci.2008.05.060

spherical flame in a confined bomb is found to be one of the most favorable, especially at high pressures [3,5–7].

In the expanding spherical flame method [3,7–14], a quiescent homogeneous combustible mixture in a closed chamber is centrally ignited and the propagating spherical flame front, $R_f = R_f(t)$, is recorded by using the Schlieren or shadow photography. When the pressure rise is negligible, the burned gas is assumed to be quiescent. As a result, the propagating velocity of the experimentally visualized flame front is equal to the flame speed with respect to the burned mixture, $S_b = dR_f/dt$. For moderate stretch rates, the flame speed can be considered to vary linearly with the stretch rate (which is $K = (2/R_f)dR_f/dt$ for expanding spherical flames) [15,16]

$$S_b = S_b^0 - L_b K \tag{1}$$

where S_b^0 and L_b are, respectively, the unstretched laminar flame speed and Markstein length with respect to the burned mixture. Therefore, S_b^0 and L_b, can be obtained from the linear extrapolation based on the plot of $S_b - K$. The laminar flame speed with respect to the unburned mixture, S_u^0, is then obtained according to the mass conservation, $S_u^0 = aS_b^0$, where $a = \rho_b/\rho_u$ is the density ratio between the burned and unburned mixtures. In the linear extrapolation, S_b and K are evaluated from the flame front history using the data range of $[R_{fL}, R_{fU}]$ [3,7–14]. The lower bound, R_{fL}, is specified to reduce the effects of initial spark ignition [10–12,17] and the upper bound, R_{fU}, is chosen to ensure that the pressure increase is negligible [7–14]. Unfortunately, different researchers made different choices without giving an appropriate justification. Sometimes, these choices were very intuitive. In our recent study [14], it was found that the data range $[R_{fL}, R_{fU}]$ can significantly affect the accuracy of flame speed measurement and great attention should be paid to choosing proper data range.

The effect of different upper bounds, R_{fU}, on the accuracy of flame speed measurement has been investigated in our previous studies [14,18]. In the current study, emphasis will be placed on the lower bound R_{fL}, which should be large enough so that the effects of ignition, flame curvature, and unsteadiness could be neglected [10–12,17]. Bradley et al. [11,12] suggested that $R_{fL} \geqslant 6$ mm in order to minimize ignition effects. Recently, Kelley and Law [19] proposed non-linear extrapolation for mixtures with large Markstein lengths. In all the previous studies [3,7–14], either linear or non-linear extrapolation is utilized. However, there is no study on how to determine the proper lower bound R_{fL} to make stretch rate small enough and radius large enough so that the linear or non-linear relationship between stretched flame speed and stretch rate is satisfied. Therefore, investigation of the mechanisms that determine the minimum lower bound R_{fL} is necessary to ensure accurate linear or non-linear extrapolation. The effects of ignition energy and unsteadiness which were only briefly discussed in [10,17], has not been systematically studied. It was shown that the flame speed changes from zero (flame ball solution) to the adiabatic planar flame speed during the propagation and the flame speed of high curved flames is one order smaller than that of planar flame due to the diffusive-controlled flame structure similar to flame ball [20]. As such, both the Lewis number of the mixture and the ignition energy will significantly affect the initial flame trajectory. Recent experimental data have shown that the flame trajectories for large Lewis number mixtures are very complicated and that using conventional extrapolation procedures for the complicated flame trajectories is difficult [19]. In order to explain discrepancies that exist among experimental data sets and provide theoretical guidance for experimental determination of flame speeds using the spherical flames, understanding how ignition energy and mixture Lewis number affect the unsteady flame evolution is important.

The objective of the present study is to examine theoretically, numerically, and experimentally the effects of Lewis number and ignition energy on front trajectories of the propagating spherical flames, and to provide a guidance for accurate determination of flame speeds by using the spherical flame experiments. First, theoretical analysis of propagating spherical flames based on the quasi-steady state assumption is presented to investigate the critical flame radius above which linear or non-linear relationship between stretched flame speed and stretch rate is satisfied for different Lewis numbers. Second, the effect of unsteady flame transition at different ignition energies is demonstrated by detailed numerical simulations. Finally, experiments on outwardly propagating spherical H_2/air flames are conducted to validate the theoretical and numerical results.

2. Theoretical analysis

The problem of outwardly propagating spherical flames has been extensively studied by using asymptotic techniques [20–26]. Ronney and Sivashinsky [21] studied the expanding spherical flames within the framework of a slowly varying flame (SVF) theory. While reasonable predictions for Lewis number (Le) less than unity were obtained, the results of the SVF theory are found to be physically unrealistic for $Le > 1$. Bechtold and coworkers [22,23] investigated the hydrodynamic and thermal-diffusion instabilities and effects of radiative loss in self-extinguishing and self-wrinkling flames. Frankel and Sivashinsky [24] examined the thermal expansion effect in

propagating spherical flames at the limit of $Le \to 1$. Chung and Law [25] conducted integral analysis for propagating spherical flames at $Le = 1$. All the above studies were based on the assumption of large normalized flame radius ($R = R_f/\delta \gg 1$, where δ is the flame thickness of adiabatic planar flame). Only the recent work by He [26] and Chen and Ju [20] spanned all the spherical flame sizes and transitions between flames at small radii (flame kernel, flame ball, and self-extinguishing flame) and large radii (propagating spherical and planar flame). Therefore, theoretical results in [20] are utilized here to investigate the critical flame radius above which linear or non-linear relationship between stretched flame speed and stretch rate is satisfied. It should be noted that the quasi-steady assumption is used and the effect of unsteadiness in the flame coordinate is not included.

The theoretical results are only briefly presented below due to the space limitations (the details could be found in [20]). By neglecting radiative loss, the relationship between the normalized flame radius, $R = R_f/\delta$, and the normalized flame speed, $U = S_b/S_b^0$, can be expressed as

$$T_f \cdot \frac{R^{-2}e^{-UR}}{\int_R^\infty \tau^{-2}\mathrm{e}^{-U\tau}\mathrm{d}\tau} - Q \cdot R^{-2}\mathrm{e}^{-UR} = \frac{1}{Le}\frac{R^{-2}\mathrm{e}^{-ULeR}}{\int_R^\infty \tau^{-2}\mathrm{e}^{-ULe\tau}\mathrm{d}\tau} = \exp\left[\frac{Z}{2}\frac{T_f - 1}{a + (1-a)T_f}\right] \quad (2)$$

where T_f, Q, and Z are, respectively, the normalized flame temperature, ignition power at the center, and Zel'dovich number. Equation (2) is valid for flames with both small and large radii. Hereafter, we refer to it as the detailed model (DM).

For flames of large radius ($R \gg 1$), the detailed model reduces to the simplified model (SM)

$$\left(U + \frac{2}{R}\right)\ln\left(U + \frac{2}{R}\right) = \frac{Z}{R}\left(\frac{1}{Le} - 1\right) - \frac{2}{R}\left(\frac{1}{Le} - 1\right) \quad (3)$$

which is similar to the theory presented in [24]. The only difference between Eq. (3) and the relation from [24] is the additional curvature term on the right hand side of Eq. (3), which was not considered in [24] for $Z \to \infty$ and $Le \to 1$. Unfortunately, for most mixtures, the Zel'dovich number is in the range of $5 \sim 15$ and the deviation of Lewis number from unity can be of order 1. As a result, the curvature term in Eq. (3) cannot be neglected. For weakly stretched flames, the stretched flame speed is nearly the adiabatic unstretched flame speed (i.e. $U = 1 + \varepsilon$ with $\varepsilon \ll 1$). In this limit, Eq. (3) reduces to the linear model (LM) (also see Eq. (1)) [15,16]

$$U = 1 - Ma \cdot Ka \quad (4)$$

where $Ka = 2U/R = K\delta/S_u^0$ is the Karlovitz number and $Ma = Le^{-1} - (Z/2)(Le^{-1} - 1)$ the Markstein number which is the same as that derived for premixed counterflow flames [27].

The normalized flame speed predicted as a function of flame radius and the Karlovitz number (in Fig. 1(b) and Fig. 5(b), $Ka = 2U/(aR)$ is used since the propagating speed, thus the flame stretch, is $1/a$ times of the laminar flame speed, S_u^0, to the zeroth order) by DM, SM, and LM for $Z = 10$, $a = 0.15$ and $Le = 0.5$, 1.0, 2.0 is shown in Fig. 1. It is observed that SM and LM only agree well with DM at large flame radius. In addition, the difference among the predictions from DM, SM, and LM strongly depends on the Lewis number. Figure 1(b) reveals that for each Lewis number, there is a critical Karlovitz number above which spherical flame cannot exist, due to the quenching caused by the coupling of flame curvature and stretch [20]. The maximum Karlovitz number for $Le = 2$ is much smaller than that of $Le = 0.5$ and 1.0, indicating that small spherical flames does not exist at large Lewis numbers due

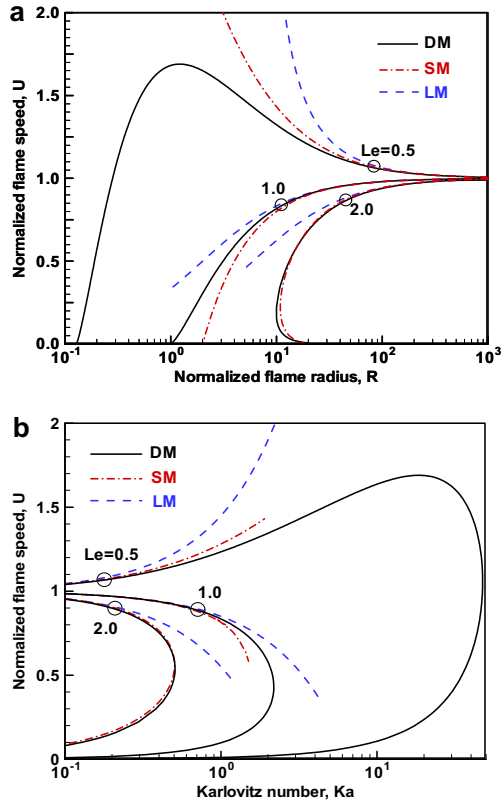

Fig. 1. Normalized flame speed as a function of (a) flame radius and (b) Karlovitz number predicted by different models for different Lewis numbers.

to the stretch effect. Finite flame curvature always decreases the flame speed (Eq. 2). However, the effect of flame stretch on flame speed depends strongly on the Lewis number derivation from unity [27]. As a result, the critical Karlovitz number, denoted by the turning points in Fig. 1(b), decreases significantly with the increase of Lewis number. As shown later, this conclusion plays an important role in determining the experimental data range for flame speed measurement.

Figure 2 shows the critical flame radius, above which the relative discrepancies between LM and DM and between SM and DM are less than 5%. Figure 2 reveals that the critical flame radius of SM is much smaller than that of LM at a given Lewis number, which is consistent with the fact that the SM is more comprehensive than the LM (SM is based on the assumption of large flame radius; while LM is based on the assumption of small stretch rate as well as large flame radius). The non-monotonic change of the critical flame radius with Lewis number is due to the fact that the absolute value of Markstein length becomes smallest when *Le* is close to a critical value which is slightly less than unity [27].

By comparing the three different models of DM, SM and LM given by Eqs. (2)–(4), we can obtain the critical flame radius above which linear or non-linear relationship between stretched flame speed and stretch rate is satisfied. This critical flame radius can be used as a guide to choose the experimental data range to determine the flame speed by using either linear or non-linear fitting approaches using Eq. 3 or 4. Since the critical flame radius changes greatly with Lewis number, for mixtures such as rich hydrogen/air or lean propane/air with Lewis numbers greatly different from unity, the lower flame radius bound R_{fL} should be specified above the critical radius so that the linear (based on LM) or non-linear (based on SM) extrapolation could be conducted.

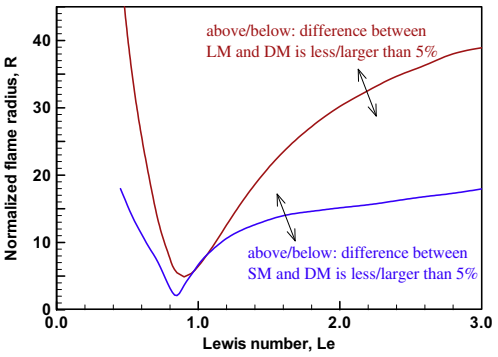

Fig. 2. The critical flame radius above which the relative discrepancies between LM and DM and between SM and DM are less than 5% at different Lewis numbers.

3. Numerical simulation

3.1. Numerical methods

In order to study the effects of unsteady flame evolution at different ignition energies, a time-accurate and space-adaptive numerical solver for Adaptive Simulation of Unsteady Reacting Flow, A-SURF (1D), has been developed to carry out high-fidelity numerical simulations of outwardly propagating spherical flames [34]. The conservation equations for a multi-species reactive mixture in a one-dimensional spherical coordinate are solved by using the finite volume method. Detailed H_2/air chemistry [28] is used in the simulation. The thermodynamic and transport properties are evaluated by using the CHEMKIN and TRANSPORT packages [29]. To maintain adequate numerical resolution of the moving flame, a multi-level, dynamically and locally adaptive mesh refinement algorithm has been developed [30]. Seven grid levels are utilized and the moving reaction zone is always fully covered by a mesh size of 16 μm. A-SURF (1D) has been successfully used in our previous studies [14,30,33]. The details on the governing equations, numerical schemes, and code validation are given in Supplementary document.

In all simulations, the spherical chamber radius is set to be $R_0 = 100$ cm and the flame trajectory data with flame radius less than 5 cm are utilized. Therefore, both the pressure increase (<1‰) and the compression-induced flow effect [14] are negligible. The flame is initiated by a small hot pocket of the burned product surrounded by fresh mixture at room temperature and pressure ($T_0 = 298$ K, $P_0 = 1$ atm). The size of the hot pocket, R_h, is between 0.9 and 2.0 mm, which changes with the equivalence ratio of H_2/air (for very rich case, which has high Lewis number, a large hot pocket is needed to obtain propagating spherical flame [33]). In order to examine the effect of ignition energy on flame trajectories, at a fixed equivalence ratio, three different hot pocket sizes, R_h, $1.2R_h$, $1.4R_h$, are utilized to mimic the experiments with different ignition energies. In the simulation, the position of flame front, R_f, is defined as the position of maximum heat release and the flame speed is calculated from the flame front history according to $S_b = dR_f/dt$.

3.2. Results and discussion

The outwardly propagating spherical H_2/air flames at different equivalence ratios ($\varphi = 0.5$, 1.0, 2.0, 3.0, 3.5, 4.0, 4.5, 5.0, 5.5) and different ignition hot pocket sizes are simulated by using A-SURF (1D). Figure 3 shows the flame speed with respect to the burned mixture, S_b, as a function of the flame radius, R_f, and flame stretch rate, *K*. The results reveal that the initial unsteady

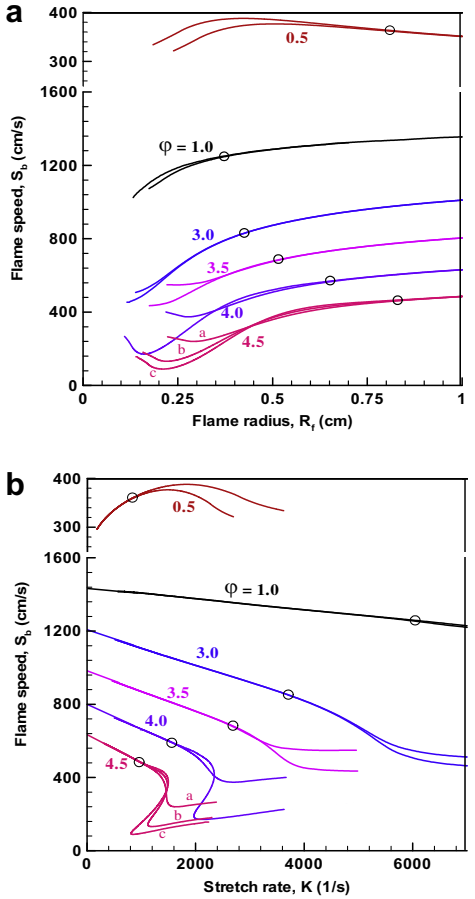

Fig. 3. Flame speed as a function of (a) flame radius and (b) stretch rate for H_2/air at different equivalence ratios: results from simulation.

flame transition and different ignition energies (hot pocket sizes) lead to different flame speed trajectories. Only above a critical flame radius, *Rc*, which is denoted by the open circles in Fig. 3, does the flame speed trajectory become independent of the ignition energy and converge to a low-dimensional manifold. With the increase of equivalence ratio, this critical flame radius increases dramatically. For $\varphi = 4.5$, the critical radius is even larger than 0.8 cm, which lies within typical experimental data ranges using for extrapolation of flame speed measurements. For example, lower flame radius bounds, R_{fL}, of 0.5 or 0.6 cm are often employed [2,7,9–12]. Therefore, additional care is needed to fit the experimental data for mixtures with a large Lewis number. Moreover, Fig. 3(b) shows that for flame radii larger than the critical radius (stretch rates less than the critical stretch rate marked by the open circles), S_b changes linearly with K, except for very small Lewis number (the lean case at $\varphi = 0.5$). As a result, for these conditions, the linear extrapolation can be utilized to obtain unstretched flame speed.

The critical radius and the Lewis number (in [27,31]) for H_2/air flames at different equivalence ratio are shown in Fig. 4. It is seen that the critical radius changes non-monotonically with the equivalence ratio and is smallest for $\varphi = 2$, which corresponds to the largest laminar flame speed and the smallest flame thickness. The non-monotonic trend between the critical radius and equivalence ratio is similar to that between flame thickness and equivalence ratio. This is caused by the fact that the duration of initial flame transition period (which is proportional to critical radius) strongly depends on the flame thickness.

In order to understand the cause for strong flame trajectory dependence on the ignition energy and Lewis number, the dependence of normalized flame speed on the Karlovitz number ($Ka = K\delta/S_u^0$) of spherical H_2/air flames is shown in Fig. 5(a). The maximum Karlovitz number changes greatly with the equivalence ratio, or more accurately, with the Lewis number. This predicted dramatic change of the maximum Karlovitz number is consistent with the theoretical prediction shown in Fig. 1(b). To show the effects of ignition energy, the theoretical results for mixture with $Le = 2$ are shown in Fig. 5(b) for comparison. Theory predicts that the ignition energy does not affect the flame trajectories above the turning point of maximum Karlovitz number. This is due to the fact that the energy deposition is treated as a boundary condition at the center and the unsteadiness is not included in the asymptotic theory [20]. However, contrary to the theory, Fig. 5(a) shows that there is a strong unsteady effect near the maximum Karlovitz number. Due to the unsteady effect, the flame speed trajectory depends on the ignition energy. For $\varphi = 4.5$, the simulations reveal that, at large Karlovitz numbers, flames initiated by large ignition energies have higher flame speeds. However, near the max-

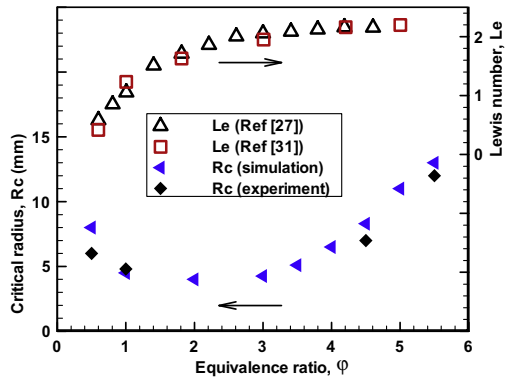

Fig. 4. Critical flame radii and Lewis numbers for H_2/air at different equivalence ratios.

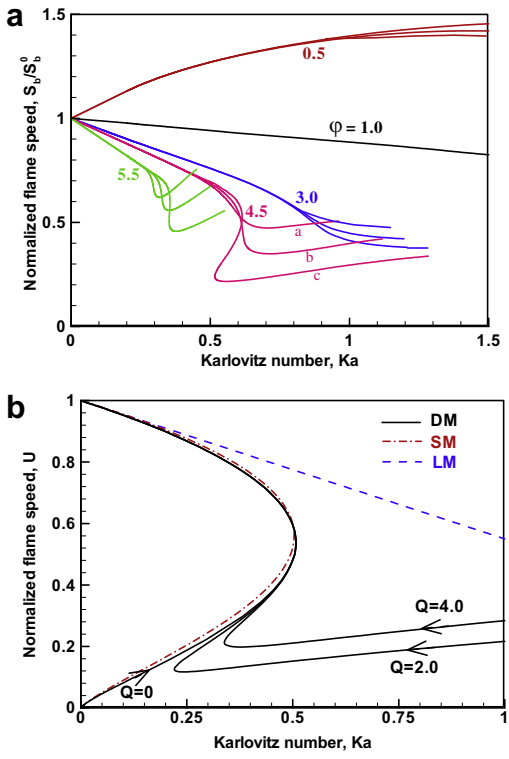

Fig. 5. Normalized flame speed as a function of Karlovitz number: (a), from simulation of H_2/air for different equivalence ratios and ignition hot pocket sizes; (b), from theory for $Le = 2.0$ and different ignition powers, Q.

imum Karlovitz number, flames with smaller ignition energy have larger flame speed. This "flame speed reverse" originates from the unsteady flame evolution near the adiabatic extinction limit (the point of maximum Karlovitz number in Fig. 5(a) and Fig. 1(b)). Because of the existence of the reverse effect at large Lewis numbers, neither non-linear fitting nor linear fitting of experimental data for flame speed determination is correct. Ignition energy and transient flame evolution significantly affect the flame trajectories and thus must be considered.

For flame radii larger than the critical radius (Fig. 3) flame speed becomes only dependent on the Karlovitz number. The critical radius above which the unsteady flame transition ends, can be found by observing the change of flame thickness during the flame propagation. Figure 6 shows the history of flame thickness (defined as the distance between the cold, $T = 400$ K, and hot, $T = 1000$ K, sides of the flame) during flame propagation for H_2/air at $\varphi = 4.5$ initiated from three different ignition hot pocket sizes (cases a, b, c, marked also in Figs. 3 and 5). The results indicate that there is a significant change in flame thickness

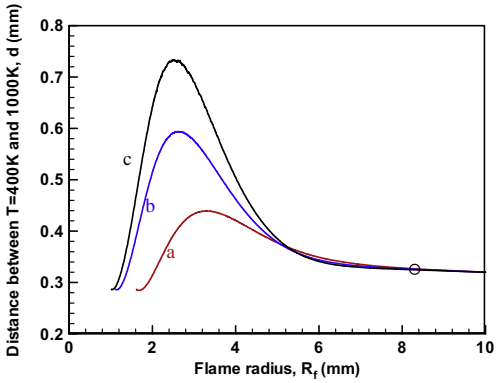

Fig. 6. Variation of flame thickness during flame propagation from different initiation kernels for H_2/air ($\varphi = 4.5$).

during the initial unsteady flame transition period. The substantial thickening of the flame initiated by the lowest ignition energy before it reaches the maximum Karlovitz number is the cause of the flame speed reverse. After the transition period, the flame thickness is almost constant and the three lines merge together onto the low-dimensional manifold for $R_f > Rc$. The change of flame thickness during the flame propagation clearly demonstrates the effect of unsteadiness on flame trajectory. In addition to the above results obtained under atmospheric conditions, numerical simulations of H_2/air flames at elevated pressures have also been conducted [34]. It is found that the flame speed reverse effect also exists at high pressures and that the critical radius decreases with pressure [34].

4. Experimental validation

4.1. Experimental methods

The experiments on propagating hydrogen/air flames are conducted in a high pressure combustion facility at normal gravity. The experimental methods are similar to our earlier work [3,18] and will be described briefly here. Pre-mixtures are prepared by using the partial pressure method from pure hydrogen, oxygen and nitrogen compressed gas sources. The combustible mixture is spark-ignited at the center of the chamber with different spark ignition energies. To study the ignition/unsteady effect, experiments on H_2/air at fixed equivalence ratio but different ignition energies (obtained by changing the voltage and spark distance for spark ignition) have been conducted. The flame propagation sequence is imaged with Schlieren photography using a high-speed digital video camera.

From the Schlieren images, the flame front is located and recorded using an automated detection program for ease of processing and reduction

of human bias. The raw flame radius data are smoothed and flame front velocity calculated using local second order polynomials fit by least-squares methods over a range of 3 mm surrounding each point. The data processed in this manner are consistent with the raw data as well as data processed through a more conventional local-averaging (low-pass) filter [18].

4.2. Results and discussion

Experiments on H_2/air flames at different equivalence ratio ($\varphi = 0.5$, 1.0, 4.5, 5.5) and different ignition energies have been conducted. Figure 7 shows the flow-corrected flame speed ($S_b = dR_f/dt$) using the methodology described in [18] as functions of flame radius and stretch rate for H_2/air for $\varphi = 4.5$. The experimental data show that the flame trajectory is strongly dependent on the ignition energy due to the unsteady flame transition. This result is consistent with the theory and the detailed numerical simulation. In addition, the existence of the flame speed reverse effect is also shown by the experimental data. Only above a critical flame radius, Rc, do the different flame speed trajectories converge onto a single curve, which corresponds to the attractive low-dimensional manifold, and thus the effect of initial flame transition can be neglected. Similar experimental results have also been reported for expanding spherical H_2/air flames at $\varphi = 5.1$ by Kelley et al. [32]. It is shown that only when the flame radius is larger than $Rc = 11$ mm (Fig. 4(b) in [32]), the $S_b - R_f$ is independent of the initial flame transition under different ignition energies. When the flame radius is larger than the critical radius, the flame speed, S_b, varies linearly with the stretch rate, K, as shown in Fig. 7. Therefore, linear extrapolation can be utilized to obtain unstretched flame speed.

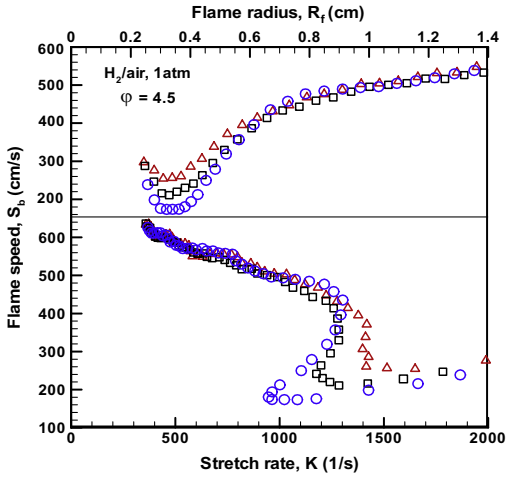

Fig. 7. Measured flame speed as functions of flame radius and stretch rate for H_2/air at $\varphi = 4.5$.

The critical radius measured from experiments is shown in Fig. 4 to compare with that from detailed numerical simulations. It is seen that the experimental results agree well with those from simulation. For stoichiometric H_2/air, the critical radius, Rc, is 5 mm; for rich H_2/air, the measured critical radii are 7 mm and 12 mm for $\varphi = 4.5$ and $\varphi = 5.5$, respectively. The lower bound, R_{fL}, should be chosen larger than the critical radius, Rc, to prevent the effect of initial flame transition. R_{fL} depends strongly on the equivalence ratio of H_2/air, and it can be larger than 10 mm for rich H_2/air. In this case, the lower bound $R_{fL} \geqslant 6$ mm, suggested in [11,12] in order to minimize ignition effects, would be too small.

5. Conclusions

In the present work, the trajectories of outwardly propagating spherical flames initiated by an external energy deposition are studied by using asymptotic theory as well as detailed numerical simulations and experiments on hydrogen/air flames. Theoretical analysis reveals a critical flame radius only above which is the linear or non-linear extrapolation for flame speeds valid. It is found that the critical radius changes non-monotonically with the Lewis number. At large Lewis numbers, the critical radius can be larger than the minimum flame radius used in the experimental measurements, leading to invalid flame speed extrapolation. The results also show that there is a critical Karlovitz number beyond which a spherical flame cannot exist, due to the quenching caused by the combined effects of flame curvature and stretch. Furthermore, both the numerical simulations and experiments show that the ignition energy has a significant impact on the flame trajectory. It is found that the unsteady flame transition at different ignition energies causes a flame speed reverse phenomenon near the maximum Karlovitz number. The occurrence of flame speed reverse greatly narrows the experimental data range for flame speed extrapolation.

Acknowledgments

This work was partially supported by the Air Force Research (F49620-04-1-0038), the U.S. Department of Energy (DE-FG26-06NT42716), and the Petroleum Research Fund from American Chemistry Society (PRF# 43460-AC5).

Appendix A. Supplementary data

Supplementary data associated with this article can be found, in the online version, at doi:10.1016/j.proci.2008.05.060.

References

[1] C.K. Law, C.J. Sung, H. Wang, T.F. Lu, *AIAA J.* 41 (2003) 1629–1645.
[2] J.T. Farrell, R.J. Johnston, I.P. Androulakis, *SAE Paper* (2004) 01–2936.
[3] X. Qin, Y. Ju, *Proc. Combust. Inst.* 30 (2005) 204–233.
[4] G.E. Andrew, D. Bradley, *Combust. Flame* 18 (1972) 133–153.
[5] C.J. Rallis, A.M. Garforth, *Prog. Energy Combust. Sci.* 6 (1980) 303–329.
[6] M. Metghalchi, J.C. Keck, *Combust. Flame* 38 (1980) 143–154.
[7] S.D. Tse, D.L. Zhu, C.K. Law, *Proc. Combust. Inst.* 28 (2000) 1793–1799.
[8] D.R. Dowdy, D.B. Smith, S.C. Taylor, A. Williams, *Proc. Combust. Inst.* 23 (1990) 325–332.
[9] S. Kwon, L.K. Tseng, G.M. Faeth, *Combust. Flame* 90 (1992) 230–246.
[10] L.K. Tseng, M.A. Ismail, G.M. Faeth, *Combust. Flame* 95 (1993) 410–426.
[11] D. Bradley, P.H. Gaskell, X.J. Gu, *Combust. Flame* 104 (1996) 176–198.
[12] D. Bradley, R.A. Hicks, M. Lawes, C.G.W. Sheppard, R. Woolley, *Combust. Flame* 115 (1998) 126–144.
[13] Z. Chen, X. Qin, Y. Ju, Z. Zhao, M. Chaos, F.L. Dryer, *Proc. Combust. Inst.* 31 (2007) 1215–1222.
[14] Z. Chen, M.P. Burke, Y. Ju, *Combust. Theory Modell.* (2008), submitted for publication.
[15] G.H. Marstein, *Non-Steady Flame Propagation*, Pergamon, New York, 1964.
[16] P. Clavin, *Prog. Energy Combust. Sci.* 11 (1985) 1–59.
[17] B. Lewis, G. Von Elbe, *Combustion Flames and Explosive of Gases*, Second ed., Academic Press, New York, 1961.
[18] M.P. Burke, Z. Chen, Y. Ju, F.L. Dryer, *Combust. Flame* (2008), submitted for publication.
[19] A.P. Kelly, C.K. Law, Fall Technical Meeting: Eastern States Sections of the Combustion Institute, Virginia, 2007, Paper B-11.
[20] Z. Chen, Y. Ju, *Combust. Theory Modell.* 11 (2007) 427–453.
[21] P.D. Ronney, G.I. Sivashinsky, *SIAM J. Appl. Math.* 49 (1989) 1029–1046.
[22] J.K. Bechtold, M. Matalon, *Combust. Flame* 67 (1987) 77–90.
[23] J.K. Bechtold, C. Cui, M. Matalon, *Proc. Combust. Inst.* 30 (2005) 177–184.
[24] M.L. Frankel, G.I. Sivashinsky, *Combust. Sci. Technol.* 31 (1983) 131–138.
[25] S.H. Chung, C.K. Law, *Combust. Flame* 72 (1988) 325–336.
[26] L. He, *Combust. Theory Modell.* 4 (2000) 159–172.
[27] C.K. Law, *Combustion Physics*, Cambridge University Press, New York, 2006.
[28] J. Li, Z. Zhao, A. Kazakov, F.L. Dryer, *Int. J. Chem. Kinet.* 36 (2004) 566–575.
[29] R.J. Kee, F.M. Rupley, J. Miller, Report No. SAND89-8009B, Sandia National Laboratories, 1989.
[30] Z. Chen, X. Qin, B. Xu, Y. Ju, F. Liu, *Proc. Combust. Inst.* 31 (2007) 2693–2700.
[31] G. Joulin, T. Mitani, *Combust. Flame* 40 (1981) 235–246.
[32] A. Kelley, G. Jomaas, C.K. Law, *AIAA*-2008-1054.
[33] Z. Chen, M.P. Burke, Y. Ju, *AIAA*-2008-0977.
[34] Z. Chen, *Studies on the Initiation, Propagation, and Extinction of Premixed Flames*, Ph.D. thesis, Princeton University, 2008.